Size Dependence of Magnetic and Optical Properties of Co_3O_4 Nanoparticles

A.K. Sarfraz* and S.K. Hasanain
Department of Physics, Quaid-i-Azam University, Islamabad, Pakistan

(Received March 28, 2013; in final form October 10, 2013)

The effect of particle size on the magnetic and optical properties of cobalt oxide Co_3O_4 has been investigated. Single phase Co_3O_4 nanoparticles were synthesized by co-precipitation route and their structure was confirmed through X-ray diffraction analysis. The average crystallite sizes of the nanoparticles as determined from the X-ray diffraction were found to lie in the range of 13 to 59 nm. At room temperature these particles show paramagnetic response and the DC magnetic moment of the samples showed an increasing trend with increasing particle size. Both the antiferromagnetic Néel temperature T_N and the low temperature moment depict finite size effects in the AC susceptibility measurements. The optical absorption studies show that there are two direct band gaps in Co_3O_4, the main energy band gap and a sub-band located inside the main energy gap. The values of these energy band gaps for the 45 nm particles were determined to be 3.15 and 1.76 eV, respectively. The direct band gap in these particles clearly shows a blue shift with decreasing size attributable to the quantum confinement effect.

DOI: 10.12693/APhysPolA.125.139
PACS 81.05.Gc, 61.05.cp, 75.75.−c, 78.66.−w

1. Introduction

The study of magnetic properties of nanosized particles is of great importance from basic as well as applications points of view [1, 2]. Néel had originally drawn the attention to the properties of antiferromagnetic nanoparticles (AFN). Néel suggested that AFN are likely to possess induced permanent magnetic moments, which depends on the lack of an internal structural perfection and/or surface spin unbalance [3]. Furthermore, antiferromagnetic nanoparticles have recently gained increased attention by virtue of their potential for exhibiting quantum tunneling of magnetization as well as their technological applications [4–6].

In general, magnetic oxides containing transition elements such as cobalt, manganese, or ruthenium exhibit most fascinating magnetic properties. Among these transition metal oxides, cobalt oxide is one of the most versatile ceramic materials, since it is a p-type antiferromagnetic oxide semiconductor. The Co_3O_4 nanoparticle system is considered an ideal material for the study of macroscopic magnetic quantum effects [7, 8].

A significant body of work exists on the magnetic and optical properties of Co_3O_4. In 20 nm Co_3O_4 particles [9] there was found a lowering of T_N compared to the bulk value, horizontally shifted hysteresis loops on field cooling, and a temperature independent magnetic relaxation rate below 10 K. The latter effect was ascribed to possible magnetic quantum tunneling in this system. Magnetic irreversibility effects were seen at temperatures in excess of T_N but the relaxation rate appeared to show a sharp maximum at the susceptibility peak.

*corresponding author; e-mail: sarfraz.ak1@gmail.com

In a recent study on crystallites of 30–40 nm size Co_3O_4 particles, a reduced Néel temperature of 25 K and two direct optical band gaps (3.12 and 1.77 eV) were observed and attributed to the excitations emanating from the presence of Co in two valence states +2 and +3 respectively [10]. (The Co^{3+} d states form a small sub-band within the main band gap whereas the Co^{2+} d states lie almost at the edge of the conduction band, while the valence band has a primarily O $2p$ character.) The corresponding values for the band gaps in the bulk are reported to be 2.85 and 1.70 eV. The observed blue shift in the band gap was explained as originating in the finite size effects of the nanoparticles. Thota et al. determined a value of moment per Co_3O_4 equal to 4.82 μ_B. The larger value of the moment compared to the spin only value of 3.87 μ_B was attributed by them to the presence of incomplete quenching of the orbital moment. Optical measurements on Co_3O_4 thin films [11] also show two direct band gaps. Co_3O_4 thin films are also studied [12] and obtained the direct band gaps at significantly lower values of 2.13 and 1.52 eV, respectively.

Also studies on the variation of lattice strains [13] as a function of Co_3O_4 particle size determined, in general, an increasing strain for smaller size particles in the range 7–18 nm. Using electron paramagnetic resonance (EPR) they obtained values for the electron g factor in the range 2.168–2.300 again indicating an orbital contribution to the moment. Rao et al. observed only one absorption edge that ranged from 2.160 to 2.67 eV for different sized particles.

It is apparent from the above highlights of Co_3O_4 nanoparticles that there are various studies of the optical and magnetic properties displaying dependences on the size of the nanocrystallites. More emphasis however has been on the optical properties and there is little data on how the size of particles affects the magnetic behav-

ior, aside from the usually reported lowering of T_N within nanoparticles of the same size. It appears that a systematic study of the size dependence in both the optical and magnetic aspects is needed, within the same set of particles. In particular, we are interested in studying how the size variations affect the magnetic behavior in both the paramagnetic and the antiferromagnetic regions where on the one hand the finite size effect will enhance the role of fluctuations and lower the T_N, while on the other hand the non-compensation of the surface spins is expected to lead to enhanced paramagnetic behavior.

2. Experimental

To prepare the Co_3O_4 nanoparticles 15 mL of 4.0 M KOH solution was slowly dropped into 15 mL of 1.0 M $CoSO_4{\cdot}7H_2O$ solution under vigorously stirring. After the reaction a pink coloured product was obtained that was kept with the solution for two hours. The precipitates so obtained consisted of cobalt hydroxide and potassium sulphate etc. The resulting solution was then centrifuged at 2000 rpm to separate the precursor $[Co(OH)_2]$ from the rest of the residual solvent. Washing of these precipitates was carried out 4–5 times with distilled water. After washing, the precipitates were placed in an oven at 50 °C overnight for the removal of remnant ions in the final product. The precursor was decomposed to Co_3O_4 by annealing it in air in a tube furnace at 250, 420, 550, 650, 750, and 850 °C, respectively, for 3 h [14].

3. Results and discussion

The X-ray diffraction patterns (XRD) for 3 h annealed samples at varying annealing temperatures between 250 °C and 850 °C are shown in Fig. 1. We have found the particle sizes of 13, 17, 27, 37, 45, and 59 nm. The normal cubic spinel structure of Co_3O_4 appears only after annealing the precursor. The XRD patterns indicate that the precursor $Co(OH)_2$ decomposition completes at 420 °C. The XRD patterns in above figures show that increasing thermal treatment temperature results in the intensifying and sharpening of the diffraction peaks. This indicates that the Co_3O_4 grains grow and the nanocrystal quality is improved. To estimate the average crystallite size of nanoparticles from the measured width of their diffraction curves (XRD pattern) we used the Scherrer formula

$$t = \frac{k\lambda}{B\cos\theta_B}.$$

In this equation, λ represent the wavelength of the X-ray radiation, B is the full width at half maximum of the diffraction peak (in radians) and θ_B — the Bragg angle. The sizes were calculated from the broadening of the three main peaks (200), (311), and (440). The average size of the crystallites varies from 13 to 59 ± 3 nm as determined by above method.

Magnetization studies were carried out to understand the effect of crystallite size variation on the magnetic properties of Co_3O_4. The DC magnetization of the samples as a function of applied field was studied using a commercial vibrating sample magnetometer. The data are shown in Fig. 2. All samples exhibited a paramagnetic response at room temperature with an increase in the paramagnetic moment with increase in average crystallite size. The DC susceptibility (M/H) or slope of paramagnetic lines in Fig. 2 increases with increasing the particle size. The inset of Fig. 2 shows the plot of magnetic moment versus the crystallite size at an applied magnetic field of 7 kOe for comparison. There is an almost 65% increase in the moment with increased size, from 13 to 59 nm. The increased moment with increasing size can be related to the presence of a magnetically dead or inert layer on the surfaces of magnetic nanoparticles due to the broken bonds, presence of impurities and the enhanced strains due to structural disorder. This dead layer becomes relatively insignificant as the size of the nanoparticles increases and the moment increases.

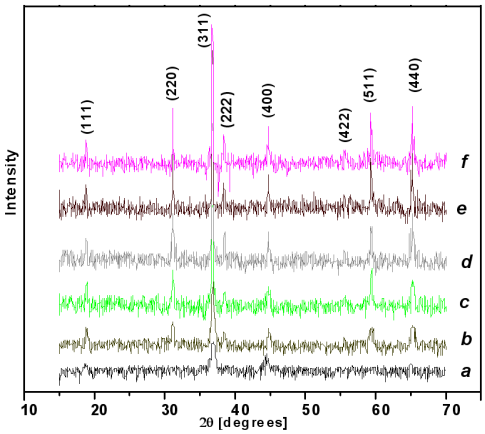

Fig. 1. XRD pattern of 3 h annealed samples of different sizes. *a* (13 nm), *b* (17 nm), *c* (27 nm), *d* (37 nm), *e* (45 nm), and *f* (59 nm).

In order to determine the Néel temperature of these antiferromagnetic nanoparticles AC susceptibility was studied in a home made susceptometer combined with a commercial closed cycle He system. The applied AC field had amplitude of 10 Oe at a frequency of 573 Hz. These measurements were performed on three different sizes, 17, 27, and 37 nm, however only the results for the 17 and 37 nm nanoparticles are being shown. The variation in the in-phase part of susceptibility $\chi(T)$ and inverse of $\chi(T)$ as function of temperature for the 37 and 17 nm samples are shown in Fig. 3a and b. An AFM is characterized by the susceptibility peak at the Néel temperature. A peak in the susceptibility was found to occur in the temperature range, $19 < T < 28$ K and $17 < T < 32$ K for the 17 nm and 37 nm nanoparticles, respectively. The peak for the larger sized particle is seen to be broader while the centre of both peaks is at about 24 K. This temperature corresponds to the Néel temperatures of the nanoparticles, whereas bulk Co_3O_4 undergoes a transition at $T_N = 40$ K

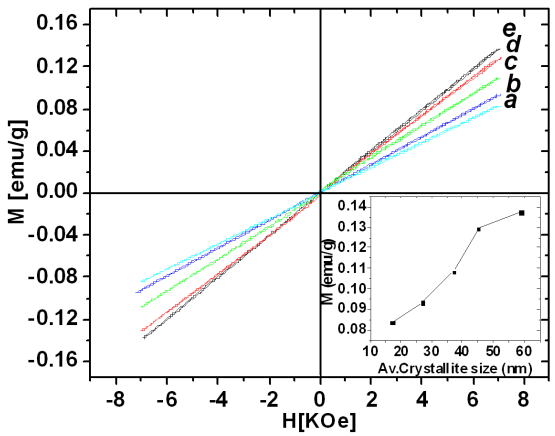

Fig. 2. Main figure: $M(H)$ behavior at 300 K for different sized samples. *a* (17 nm), *b* (27 nm), *c* (37 nm), *d* (45 nm), and *e* (59 nm). Inset: variation of moment with size ($H = 7$ kOe).

as reported in literature [15, 16]. Hence it is apparent that the particles, 17 and 37 nm, have a significantly lower Néel temperature than the bulk, and no significant difference in the Néel temperatures between the two sets of particles could be discerned from the susceptibility peaks. This value of T_{N} is lower than the reported bulk value of 40 K. The decrease in the Néel temperature for nanoparticles as compared to bulk value has been reported in the literature [17, 18]. Resnick et al. found T_{N} of 15 K for 4 nm particles [19].

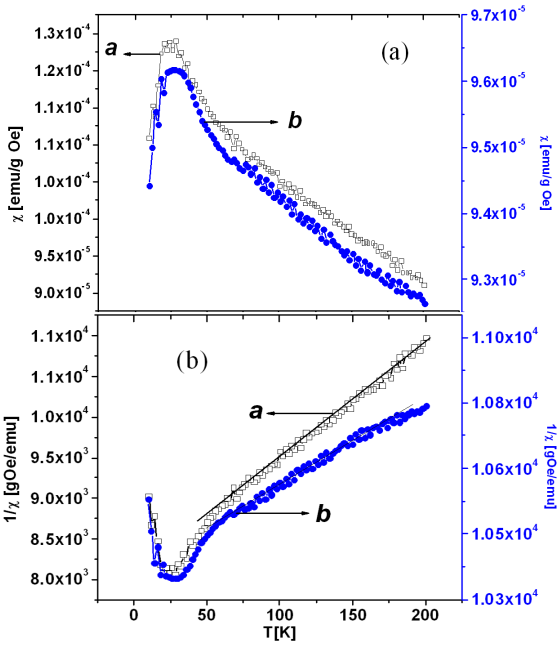

Fig. 3. (a) Temperature variation of AC susceptibility of two of the samples *a*: 17 nm and *b*: 37 nm ($h_{\mathrm{ac}} = 20$ Oe). (b) Inverse of AC susceptibility versus temperature, for the samples *a*: 17 nm and *b*: 37 nm.

An estimate of the Néel temperature can also be made from the Curie–Weiss plot. By extrapolating the inverse of susceptibility line to zero, the intersection with the T axis was seen to occur at (negative) temperatures of $\theta_{\mathrm{N}} = -26$ K and -31 K, respectively, for the above two samples of 17 nm and 37 nm nanoparticles as shown in Fig. 3a and b. The negative values of θ_{N} attained from the Curie law fit showed that the system has AFM interactions, as expected. The values of θ_{N} lie within the range of the peak temperatures in respective plots of χ. This clearly shows that the decline in χ (the peak at T_{P}) is to be attributed to the onset of the atomic force microscopy (AFM) transition. The larger value of θ for the larger sized particles is consistent with the above discussion of the role of finite size and surface effects in lowering the magnetic ordering temperatures. Interestingly, we noted that as the crystallite size decreases, the magnetic susceptibility both at the peak and below it, in the antiferromagnetic state, are higher. The peak value of susceptibility decreased systematically from 1.24×10^{-4} to 1×10^{-4} emu/g/Oe and finally to 0.96×10^{-4} emu/g/Oe as the size increased from 17 to 27 and finally to 37 nm particles.

Furthermore, below the peak (e.g. at 10 K) we find a similar trend in the decrease of the susceptibility from 1.1×10^{-4} to 0.94×10^{-4} emu/g/Oe as the size increased from 17 to 37 nm particles. It is apparent that this trend is in contrast to that observed at room temperature where the larger sized particles had a larger paramagnetic moment. The trend at lower temperatures can be understood in terms of the increasing finite size effects in smaller particles that will tend to destabilize antiferromagnetic alignments as the temperature approaches and decreases below T_{N}.

In addition to the enhanced role of thermal fluctuations in destabilizing the antiferromagnetic alignment in smaller particles, the role of surface spin disorder is also to be considered. The structural disorder at the surface is understood to lead to spin disorder [20] leading at low temperatures to incomplete antiferromagnetic alignment and in a larger moment. The non-compensation of the antiferromagnetic moment because of the increased role of surface spin disorder increases as the nanoparticle size decreases (surface-to-volume ratio increases). This observation indicates that it is possible that the observed decrease in the Néel temperatures of the particles (as compared to the bulk) could also be due to the presence of the uncompensated spins that may create a magnetic moment destabilizing the AFM state.

From the slope of the $1/\chi$ vs. T data we determined the value of the Curie constant ($C = N\mu_{\mathrm{eff}}^2 3k_{\mathrm{B}}$) equal to 2.3×10^{-2} K emu/(g Oe). Using the value of N, the number of Co atoms per g, as equal to $N = 7.49 \times 10^{21}$, we obtain $\mu_{\mathrm{eff}} = 3.487 \times 10^{-20}$ emu. This converts to $\mu_{\mathrm{eff}} = 3.73\ \mu_{\mathrm{B}}$/Co.

Various values have been quoted for μ_{eff}/Co. Dutta et al. [15] have reported an experimental value of 4.09 μ_{B} while others [21, 10] have obtained values of 3.26 μ_{B},

and 4.82 μ_B/Co. Larger values of the effective moment than expected from spin only contribution (3.87) are attributed to the non-vanishing of the orbital component of angular momentum for the Co^{2+} ions (the Co^{3+} ions are in low spin state with $S = 0$, and hence only the Co^{2+} contribute to the moment).

In order to understand the band structure of Co_3O_4 nanoparticles and to determine the effect of crystallite size on band gap energies, we conducted optical absorption spectroscopy. There are two direct band gap transitions in bulk Co_3O_4 in the range 1.88–2.13 eV and 1.50–1.52 eV, respectively [11, 12]. The first band gap can be assigned to the O^{2-}–Co^{2+} charge transfer process while the second band gap can be assigned to O^{2-}–Co^{3+} charge transfer process. Cobalt obviously is present in both +2 and +3 states to provide a total of eight electrons to each formula unit.

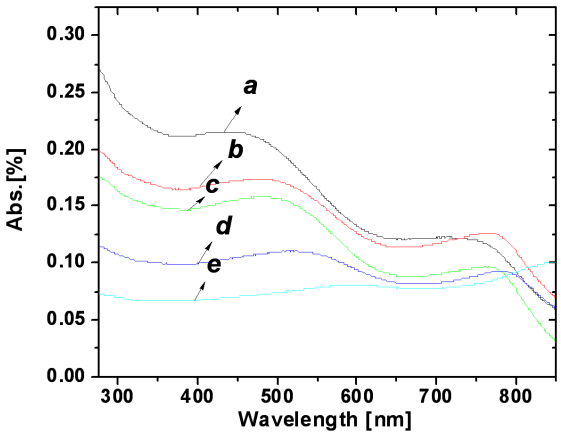

Fig. 4. Absorption spectra of different sized samples. *a* (13 nm), *b* (17 nm), *c* (27 nm), *d* (37 nm), and *e* (45 nm).

Optical absorption spectra of the samples of 13 nm to 45 nm particles were taken at room temperature by dispersing them in absolute ethanol which is a low absorbing medium. To cancel the effect (if any) of absolute ethanol, 0% absorbance baseline was set using absolute ethanol. All spectra were taken in the range 250–1000 nm on Lemda-950 Perkins Elmer double beam spectrometer with quartz cuvettes of dimensions $1 \times 1 \times 4.5$ cm^3 as the holders for the sample and reference solutions. Absolute ethanol was used as the reference solution. UV-Vis absorption spectra of the samples mentioned above are shown below in Fig. 4. To estimate the value of the direct band gap of Co_3O_4 nanoparticles from the above absorption spectra we used the following equation [22, 23]:

$$(\alpha h\nu)^n = B(h\nu - E_g), \tag{1}$$

where $h\nu$ is the photon energy in eV, α is the absorption coefficient in cm^{-1}, B is a constant related to the material, while the value of $n = 2$ for direct transitions, as in our case. To calculate α, we needed the transmittance T which was calculated using the Beer–Lambert law [24]:

$$A = -\log_{10}(T). \tag{2}$$

Here A represents absorbance and T the absolute value of the transmittance. By measuring the absorbance A the transmittance T was determined from Eq. (2). The absorption coefficient α was calculated using the relation

$$\alpha d = \ln(1/T). \tag{3}$$

In this expression d is the thickness of the sample in units of centimeters (cm), and was taken as the cuvette length. Using these values in Eq. (1) the value of e_g was determined using different values of n. The best linear fit was obtained by plotting $(\alpha h\nu)^2$ against photon energy ($h\nu$), indicating that the absorption edges are due to a direct allowed transitions. The linear fit to the $(\alpha h\nu)^2$ versus $h\nu$ plot was obtained by fitting a straight line to the linear portion of the curve. The value of optical absorption edges has been determined from the value of intercepts of the straight line at zero of the ordinate.

Figure 5 below shows the direct band gap estimation due to O^{2-}–Co^{3+} and O^{2-}–Co^{2+} charge transfer processes for 37 nm particles. Values of the band gaps for the other samples were determined similarly.

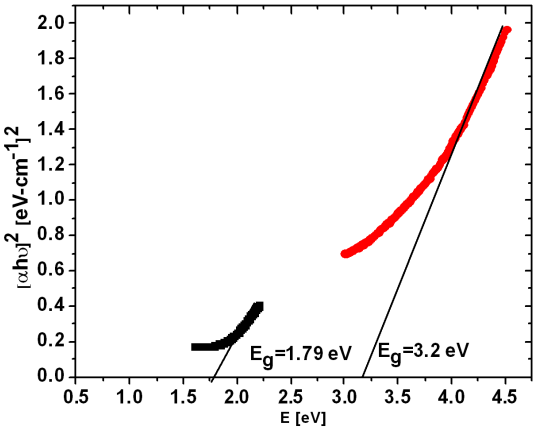

Fig. 5. Estimation of direct band gaps for the 37 nm sample from data of Fig. 4 using Eq. (1) of text. The transitions are due to the O^{2-}–Co^{3+} and O^{2-}–Co^{2+} charge transfer.

Graphical representation of band gap variation with crystallite size for the above mentioned samples due to O^{2-}–Co^{3+} and O^{2-}–Co^{2+} charge transfer processes is shown in Fig. 6. From Fig. 6, a clear blue shift in direct band gaps can be observed with decrease in the crystallite size in our samples. Such a blue shift for Co_3O_4 has been variously reported in the literature [25]. The value of the band gaps for the bulk material are reported to be 1.7 eV and 2.85 eV for the transitions from the valence band to the Co^{3+} and Co^{2+} subbands, respectively. We note that the values for both the band gaps increase with decreasing size. The band gap for the O^{2-}–Co^{3+} transition varies from 1.76 to 1.92 ($\pm$0.03) eV as the size varies from 45 nm to 13 nm. In the same size range the band gap for the O^{2-}–Co^{2+} transitions varies from 3.15 to 3.40 ($\pm$0.04) eV. It is noticeable that while for the lower

O^{2-}–Co^{3+} transition the band gap has almost attained the bulk value (1.70 eV) for the largest size of 45 nm, the O^{2-}–Co^{2+} transition is still significantly higher than for the bulk.

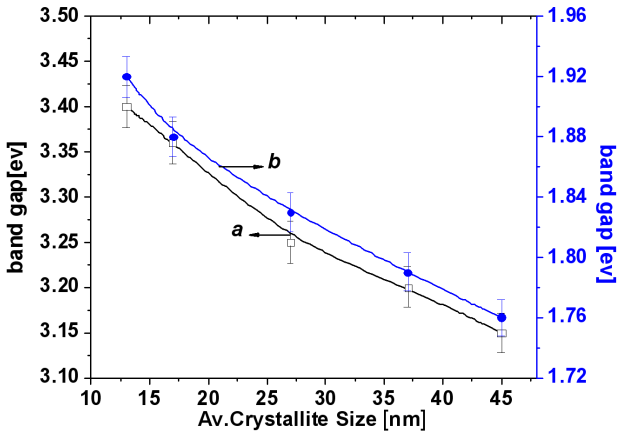

Fig. 6. Graphical representation of direct band gap variation with crystallite size. *a*: O^{2-}–Co^{2+}; *b*: O^{2-}–Co^{3+} charge transfer processes. Curves are guide to the eye.

Rao et al. [13] find a value of the smaller gap varying between 2.16 eV and 2.67 eV for sizes varying between 7 and 18 nm while Thota et al. [10] obtained values of 3.12 eV and 1.77 eV for the respective energy gaps for 20 nm average size particles. The blue shift in the band gaps for nanosized particles is understood to be due to the quantum confinement effect [26]. Therefore the presence of a blue shift in both the band gaps as compared to the bulk Co_3O_4 as well as the increase in the band gap with decreasing size in the range of 13–45 nm is clear evidence that these particles are well within the strong confinement regime. The larger amount of blue shift for the O^{2-}–Co^{2+} transitions as compared to those for the O^{2-}–Co^{3+} transitions suggests that for the ions located in the tetrahedral and octahedral symmetries, respectively, the confinement effects are not identical.

4. Conclusion

We have compared the magnetic and optical properties of different sized Co_3O_4 nanoparticles. The magnetic properties are affected by the finite size of the particles in the sense of a significant lowering of the Néel temperature as compared to the bulk and also a slight decrease in T_N as the size of the particles is decreased. We find that for larger sized particles the room temperature moment, far from T_N, is larger than for the smaller particles, indicating the presence of what may be regarded as a magnetically dead layer at the surface. This inert layer leads to a pronounced lowering of the paramagnetic moment for the smaller sized particles due to larger surface to volume ratio. However we find interestingly that at temperatures approaching and below T_N the susceptibility of the smaller particles is larger than that of the larger particles suggesting that the uncompensated spins in the case of the smaller particles are responsible for an incomplete cancellation of the moment and hence a larger moment and susceptibility.

Absorption spectroscopy shows a continuing increase in both the direct band gaps with the O^{2-}–Co^{2+} transition continuing to show a large difference from the bulk value of the same while the O^{2-}–Co^{2+} transition shows a smaller change and the value of the gap has almost attained the bulk value for the 45 nm particles. We suggest that the difference in the confinement effects for the two band gaps might emanate from the differences in the effective masses of the carriers in the sub-bands created by the two types of Co ions, each one being located at a different symmetry, since the band gap shift is sensitively dependant on the effective masses of the carriers.

Acknowledgments

S.K.H. acknowledges the support of Higher Education Commission Govt. of Pakistan for supporting this project of "Development and Study of Magnetic Nanostructure".

References

[1] S. Jacobs, C.P. Bean, in: *Magnetism*, Vol. III, Eds. G.T. Rado, H. Suhl, Academic Press, New York 1963, p. 294.

[2] R.W. Chantrell, K. O'Grady, in: *Applied Magnetism*, Ed. R. Gerber, Kluwer Academic, Dordrecht, Netherlands 1994, p. 113.

[3] L. Néel, in: *Low Temperature Physics*, Eds. C. Dewitt, B. Dreyfus, P.G. de Gennes, Gordon and Breach, New York 1962, p. 413.

[4] M.M. Ibrahim, S. Darwish, M. Seehra, *Phys. Rev. B* **51**, 2955 (1995).

[5] S. Gider, D. Awschalom, T. Douglas, S. Mann, M. Chaparala, *Science* **268**, 77 (1995).

[6] J. Tejada, X.X. Zhang, E. del Barco, J.M. Hernández, E.M. Chudnovsky, *Phys. Rev. Lett.* **79**, 1754 (1997).

[7] B. Barbara, E.M. Chudnovsky, *Phys. Lett. A* **145**, 205 (1990).

[8] S. Takada, M. Fujii, S. Kohiki, T. Babasaki, H. Deguchi, M. Mitome, M. Oku, *Nano Lett.* **1**, 379 (2001).

[9] A. Makhlouf, *J. Magn. Magn. Mater.* **246**, 184 (2002).

[10] S. Thota, A. Kumar, J. Kumar, *Mater. Sci. Eng. B* **164**, 30 (2009).

[11] D. Barreca, C. Massignan, S. Daolio, M. Fabrizio, C. Piccirillo, L. Armelao, E. Tondello, *Chem. Mater.* **13**, 588 (2001).

[12] A. Gulino, P. Dapporto, P. Rossi, I. Fragala, *Chem. Mater.* **15**, 3748 (2003).

[13] K.V. Rao, C.S. Sunandana, *Solid State Commun.* **148**, 32 (2008).

[14] L. He, C. Chen, N. Wang, W. Zhou, L. Guo, *J. Appl. Phys.* **102**, 103911 (2007).

[15] P. Dutta, M.S. Seehra, S. Thota, J. Kumar, *J. Phys., Condens. Matter* **20**, 015218 (2008).

[16] W.L. Roth, *J. Phys., Chem. Solids* **25**, 1 (1964).

[17] T. Ambrose, C.L. Chien, *Phys. Rev. Lett.* **76**, 1743 (1996).

[18] Y.J. Tang, D.J. Smith, B.L. Zink, F. Hellman, A.E. Berkowitz, *Phys. Rev. B* **67**, 054408 (2003).

[19] A.D. Resnick, K. Gilmore, Y.U. Idzerda, M.T. Klem, M. Allen, T. Douglas, E. Arenholz, M. Young, *J. Appl. Phys.* **99**, 08Q501 (2006).

[20] R.H. Kodama, *J. Magn. Magn. Mater.* **200**, 359 (1999).

[21] X.L. Xu, Z.H. Chen, Y. Li, W.K. Chen, J.Q. Li, *Surf. Sci.* **603**, 653 (2009).

[22] X. Wang, X. Chen, L. Gao, H. Zheng, Z. Zhang, Y. Qian, *J. Phys. Chem. B* **108**, 16401 (2004).

[23] R.K. Willardson, A.C. Beer, *Semiconductor and Semimetals: Optical Properties of III–V Compounds*, Academic Press, New York 1996.

[24] L.H.J. Lajunen, P. Peramaki, *Spectrochemical Analysis by Atomic Absorption and Emission*, Royal Society of Chemistry, UK 2004.

[25] J. Gao, Y. Zhao, W. Yang, J. Tian, F. Guan, Y. Ma, *J. Uni. Sci. Tech. (Beijing)* **10**, 54 (2003).

[26] F. Gu, C. Li, Y. Hu, L. Zhang, *J. Cryst. Growth* **304**, 369 (2007).